antioxidants

MDPI

Article

The Fate of Oxidative Strand Breaks in Mitochondrial DNA

Genevieve Trombly [1], Afaf Milad Said [1], Alexei P. Kudin [1], Viktoriya Peeva [1], Janine Altmüller [2,3], Kerstin Becker [2,4], Karl Köhrer [4], Gábor Zsurka [1,5,*] and Wolfram S. Kunz [1,5,*]

1 Institute of Experimental Epileptology and Cognition Research, Medical Faculty, University of Bonn, 53127 Bonn, Germany
2 Cologne Center for Genomics and Center for Molecular Medicine Cologne (CMMC), Medical Faculty, University of Cologne, 50923 Köln, Germany
3 Institute of Human Genetics, University of Cologne, 50923 Köln, Germany
4 Biological and Medical Research Centre (BMFZ), Genomics & Transcriptomics Laboratory, Heinrich-Heine-University Duesseldorf, 40225 Düsseldorf, Germany
5 Department of Epileptology, University Hospital Bonn, 53127 Bonn, Germany
* Correspondence: gabor.zsurka@ukbonn.de (G.Z.); wolfram.kunz@ukbonn.de (W.S.K.)

Abstract: Mitochondrial DNA (mtDNA) is particularly vulnerable to somatic mutagenesis. Potential mechanisms include DNA polymerase γ (POLG) errors and the effects of mutagens, such as reactive oxygen species. Here, we studied the effects of transient hydrogen peroxide (H_2O_2 pulse) on mtDNA integrity in cultured HEK 293 cells, applying Southern blotting, ultra-deep short-read and long-read sequencing. In wild-type cells, 30 min after the H_2O_2 pulse, linear mtDNA fragments appear, representing double-strand breaks (DSB) with ends characterized by short GC stretches. Intact supercoiled mtDNA species reappear within 2–6 h after treatment and are almost completely recovered after 24 h. BrdU incorporation is lower in H_2O_2-treated cells compared to non-treated cells, suggesting that fast recovery is not associated with mtDNA replication, but is driven by rapid repair of single-strand breaks (SSBs) and degradation of DSB-generated linear fragments. Genetic inactivation of mtDNA degradation in exonuclease deficient POLG p.D274A mutant cells results in the persistence of linear mtDNA fragments with no impact on the repair of SSBs. In conclusion, our data highlight the interplay between the rapid processes of SSB repair and DSB degradation and the much slower mtDNA re-synthesis after oxidative damage, which has important implications for mtDNA quality control and the potential generation of somatic mtDNA deletions.

Keywords: mitochondrial DNA; oxidative damage; mtDNA double-strand breaks mtDNA single-strand breaks; mtDNA degradation

check for updates

Citation: Trombly, G.; Said, A.M.; Kudin, A.P.; Peeva, V.; Altmüller, J.; Becker, K.; Köhrer, K.; Zsurka, G.; Kunz, W.S. The Fate of Oxidative Strand Breaks in Mitochondrial DNA. *Antioxidants* **2023**, *12*, 1087. https://doi.org/10.3390/antiox12051087

Academic Editor: Stanley Omaye

Received: 31 March 2023
Revised: 27 April 2023
Accepted: 10 May 2023
Published: 12 May 2023

Copyright: © 2023 by the authors. Licensee MDPI, Basel, Switzerland. This article is an open access article distributed under the terms and conditions of the Creative Commons Attribution (CC BY) license (https://creativecommons.org/licenses/by/4.0/).

1. Introduction

The idea of persistent oxidative damage of mtDNA leading to the accumulation of somatic mutations during a lifetime has led to the 'mitochondrial theory of aging' [1]. This is based on the fact that mtDNA is localized at the matrix side of the mitochondrial inner membrane—a highly oxidative environment due to the presence of iron required for heme and iron-sulfur protein synthesis [2] as well as the presence of single-electron donors within the mitochondrial respiratory chain required for the formation of reactive oxygen species (ROS) [3]. The 'mitochondrial theory of aging' concept has been challenged by later observations that the somatic mitochondrial point mutation profile of aging cells and tissues does not contain abundant G > T/C > A transversions that are considered to be the hallmark of oxidative DNA damage. Rather, abundant G > A/C > T transitions point to mitochondrial DNA polymerase γ (POLG) errors as the potential cause of the somatic mutation profile in aging [4,5]. Recent publications have accordingly paid little attention to the role of oxidative mutagenesis in somatic mtDNA mutation generation [6–8]. However, it has been noted that the missing G > T/C > A point mutation profile does not exclude profound oxidative mutagenesis of mtDNA, but can be explained by the nucleotide

selectivity of POLG, which allows 7,8-dihydro-8-oxo-20-deoxyguanosine (8oxodG, an abundant product of DNA oxidation) to pair with cytosine [9]. Additionally, the highly reactive •OH radical does not only modify bases but can also generate mtDNA single-strand breaks (SSB) or a combination of both (for a comprehensive overview of products, see [10]). This process eventually leads to double-strand breaks (DSB) which, in turn, might facilitate deletion formation. To avoid this harmful somatic mutagenesis, mitochondria contain (i) a LIG3-dependent base excision repair (BER) pathway that includes repair of single strand breaks [11], and (ii) a MGME1 and POLG exonuclease-dependent degradation pathway of linear mtDNA [12]. mtDNA degradation after oxidative stress has been suggested to circumvent the accumulation of somatic mutations leading to the idea of a 'disposable mitochondrial genome' [13,14]. However, the relative impact of repair and degradation pathways for mtDNA quality control still remains to be elucidated.

In the present report, we describe the interplay of repair, degradation and re-synthesis of mtDNA in an immortalized human embryonic kidney (HEK 293) cell model after oxidative damage by transient hydrogen peroxide treatment. We show that efficient degradation of DSB-generated linear DNA is pivotal to mtDNA quality control and ensures, together with fast repair of SSBs, effective clearance of oxidatively damaged mtDNA molecules.

2. Materials and Methods

2.1. Cell Culture

Immortalized human embryonic kidney (HEK 293) cells were commercially obtained from ATCC, catalogue Nr. CRL-1573. Cells were cultured in DMEM with GlutaMAX™ (Gibco, Paisley, UK) or stable glutamine (PAN Biotech, Aidenbach, Germany) containing high glucose (25 mM) and 1 mM sodium pyruvate. The medium was supplemented with 50 µg/mL uridine (Sigma-Aldrich/Merck, Darmstadt, Germany), 10% heat-inactivated tetracycline-free FBS (PAN Biotech, Aidenbach, Germany), and 100 U/mL penicillin and streptomycin (Gibco, New York, NY, USA). The POLGexo$^{-/-}$ cell line (p.D274A mutant) was obtained by CRISPR/Cas9 genome editing as described in Ref. [12]. The genotype was confirmed by Sanger sequencing (Figure S1).

Transient oxidative stress was induced on cells seeded at 90% confluence by applying H_2O_2 (Honeywell, Seelze, Germany) at concentrations of 0.5 or 1 mM. Viability was determined by adding 0.1% erythrosine B (Sigma-Aldrich, St. Louis, MO, USA) to cells suspended in 1× PBS (Gibco, Paisley, UK) and using a Neubauer hemocytometer (Paul Marienfeld, Lauda-Königshofen, Germany).

2.2. Measurement of H_2O_2 Decay

Time-dependent concentration changes of H_2O_2 in cell growth medium in the presence or absence of cells were determined by the fluorometric Amplex red/peroxidase-coupled method [15] using 1 µM Amplex red (Sigma-Aldrich, St. Louis, MO, USA) and 20 U/mL horseradish peroxidase (Sigma-Aldrich, St. Louis, MO, USA) at λ_{ex} = 560 nm and λ_{em} = 590 nm. For the measurement, a phenol red-free cell culture medium was used.

2.3. Total DNA Isolation

DNA was isolated from cell pellets with the QIAamp DNA mini kit (Qiagen, Hilden, Germany) according to the manufacturer's protocol for tissue isolation. DNA concentration was measured using a Qubit™ 4 fluorometer (Invitrogen/Fisher Scientific, Schwerte, Germany). Qubit™ assay tubes and a Qubit™ 1× dsDNA HS Assay Kit (Invitrogen, Eugene, OR, USA) were used according to the manufacturer's protocol.

2.4. Isolation of mtDNA

Mitochondria were isolated from whole cells via differential centrifugation based on the protocol outlined in [16]. Before mitochondria isolation, ice-cold isolation buffer (210 mM mannitol, 70 mM sucrose and 5 mM HEPES-KOH, pH = 7.2) was bubbled with argon gas (Linde, Pullach, Germany) for a minimum of 30 min to remove any oxygen

in the solution that would result in additional oxidative mtDNA damage and supplemented with 0.25% BSA (PAN Biotech, Aidenbach, Germany). The mitochondrial pellet obtained from 300 to 900 million cells was incubated with proteinase K (Qiagen, Hilden, Germany, >600 mAU/mL; 15 µL in 900 µL argon-saturated isolation buffer without BSA) at 26 °C for 1 h. Mitochondrial pellets were washed twice in BSA-containing isolation buffer and directly underwent DNA isolation using the QIAamp DNA mini kit (Qiagen, Hilden, Germany).

2.5. Southern Blot

A total of 1 µg DNA was digested with *Mlu*I-HF restriction endonuclease (New England Biolabs, Frankfurt am Main, Germany) for cleavage of nuclear DNA. This restriction endonuclease does not have a cutting site on the mitochondrial genome. DNA was separated, along with DIG-labeled DNA Molecular Weight Marker II (Roche, Mannheim, Germany), in a 0.6% agarose gel containing 1.25 µM ethidium bromide at 40 V overnight. The gels were alkaline treated and neutralized before the DNA was blotted to Zeta-Probe membranes (Bio-Rad, Hercules, CA, USA) and immobilized by baking at 80 °C for 30 min. Blots were hybridized overnight at 48 °C with PCR-generated digoxigenin-labeled probes. Probes were synthesized using the PCR DIG Probe Synthesis Kit (Roche, Mannheim, Germany) with primers 5′-TCATCCCTGTAGCATTGTTCG-3′ and 5′-GAAGAACTGATTAATGTTTGGGTCT-3′ for the *MT-ND5* gene in the region 12602–12690 in the mitochondrial genome, or primers 5′-GTTGGTGGAGCGATTTGTCT-3′ and 5′-GGCCTCACTAAACCATCCAA-3′ for nuclear 18S rRNA genes. Chemiluminescent detection with anti-DIG-AP antibody F_{ab} fragment (Roche, Mannheim, Germany) and CSPD (Roche, Mannheim, Germany) was performed, and the signal was recorded on a ChemiDoc Imaging System (Bio-Rad, Hercules, CA, USA) [12].

2.6. Assessment of the Number of mtDNA Breaks by qPCR

Quantitative PCR (qPCR) was used to determine the relative amount of damage present in mtDNA by comparing a short mtDNA product to one over a longer region of mtDNA (gene accession number: NM_001126131.2 and NP_001119603.1). Primers 3922F (5′-CTAGGAAGATTGTAGTGGTGAGGGTG-3′) and 4036R (5′-GAACTAGTCTCAGGCTTCA ACATCG-3′) were used to amplify a minor arc segment 115 bps in size, while primers 3922F together with 5625R (5′-ACACCGCTGCTAACCCCATAC-3′) amplify 1704 bps of the minor arc. Amplifications were performed in a C1000 Touch™ Thermal Cycler CFX96™ Real-Time System (Bio-Rad, Hercules, CA, USA) using Luna Universal qPCR Master Mix (New England Biolabs, Frankfurt am Main, Germany) under the following conditions: 95 °C for 15 min and 38 cycles of 95 °C for 15 s, 70 °C for 30 s and 68 °C for 4 min. Triplicate reactions were performed for three different concentrations of template DNA. C_t values were defined at the inflection points of fitted 4-parameter sigmoidal or Chapman curves. The relative frequency of breaks per molecule was calculated according to the formula $\ln(2\hat{}((C_{t[long]} - C_{t[short]}) - \Delta C_{t[ref]}))$ where $\Delta C_{t[ref]}$ is the average value of $C_{t[long]} - C_{t[short]}$ in wild-type cells before treatment. Amplification efficiency was 97.5 ± 1.4% for the short fragment and 75.5 ± 2.8% for the long fragment.

2.7. BrdU Incorporation

Incorporation of 5-bromo-2′-deoxyuridine (BrdU) into mtDNA can be used to visualize replication and repair kinetics [17]. One hour before applying BrdU to cells, aphidicolin (Merck, Darmstadt, Germany) dissolved in DMSO was added to the cell culture medium at a final concentration of 20 µM in order to allow for the halting of nuclear DNA replication [18]. Water-dissolved BrdU (Roche, Mannheim, Germany) was then added to the cell culture medium to a final concentration of 10 µM. BrdU incorporation was visualized by Southern blotting and chemiluminescent detection using an anti-BrdU primary antibody (mouse IgG, Product no: 11170376001, Merck, Darmstadt, Germany) and a goat anti-mouse HRP conjugate (Bio-Rad, Hercules, CA, USA) as a secondary antibody. The chemilumines-

cent signal was developed using the Clarity Western ECL Substrate kit (Bio-Rad, Hercules, CA, USA), and the signal was recorded on a ChemiDoc Imaging System (Bio-Rad, Hercules, CA, USA) [19].

2.8. Short-Read (Illumina) Sequencing of Linker-Ligated Isolated mtDNA

A total of 1.5 µg purified mtDNA was ligated to a one-side-blunt double-stranded linker as described in [12] and subsequently column purified with QIAamp DNA Mini Kit (Qiagen, Hilden, Germany). Libraries were prepared and size selected by using the Illumina TruSeq Nano DNA Sample Preparation Kit and Agencourt AMPure XP beads. One cycle of PCR followed to complete the library adaptor structure. Libraries were validated with the Agilent 2200 TapeStation and quantified by qPCR. An Illumina NovaSeq 6000 instrument (Illumina, San Diego, CA, USA) generated 150 bp paired-end reads. For each sample, 0.7–1.4 $\times$ 10^7 paired mitochondrial reads were obtained, representing 50–95% of all reads and resulting in 1.2–2.3 $\times$ 10^5 average coverage. Reads were aligned to sample-specific reference mitochondrial sequences and screened for the linker sequence using an in-house Perl script (available upon request). To convert potential overhangs at DSBs to ligatable blunt ends and to increase the efficiency of linker ligation, mtDNA samples were treated with T4 polymerase and polynucleotide kinase using the Quick Blunting™ Kit (New England Biolabs, Frankfurt am Main, Germany) according to the manufacturer's protocol: 1 µL of enzyme mix was used to treat 3 µg of mtDNA for 30 min at room temperature. To aid in the detection of SSBs, 350 ng mtDNA was treated with 100 U S1 nuclease (Thermo Scientific, Vilnius, Lithuania) for 15 min at 37 °C [20] before proceeding with linker ligation as described above.

2.9. PacBio Single-Molecule Long-Read Sequencing of Isolated mtDNA

For PacBio single-molecule long-read sequencing, 1.5 µg of isolated mtDNA was linearized by the single-cutter restriction endonuclease *Eag*I (New England Biolabs, Frankfurt am Main, Germany). Samples were RNase digested and purified on 0.8× AMPure PB beads prior to library preparation with the Express Template 2.0 kit (Pacific Biosciences, Menlo Park, CA, USA)—according to the protocol "Procedure & Checklist—Preparing Multiplexed Microbial Libraries Using SMRTbell Express Template Prep Kit 2.0" (Version 04, November 2019)—without additional DNA shearing, starting with the removal of single-strand overhangs, and using the Barcoded Overhang Adapter Kit 8A or B (Pacific Biosciences) for adapter ligation. After library preparation, six libraries were pooled equimolarly, and the pools' size selected with diluted AMPure PB beads to remove fragments <3 kb. Library pools were quantified (Qubit) and analyzed for final fragment size distribution (Fragment Analyzer, Agilent, Santa Clara, CA, USA). Sequencing primers and polymerase were successively annealed and bound to the libraries, and each pool was sequenced on one 8M SMRT cell on a Sequel II Instrument (Pacific Biosciences, Menlo Park, CA, USA) with 30 h movie time and 2 h pre-extension. Circular consensus sequence reads were generated and demultiplexed with SMRT Link v9 (Pacific Biosciences, Menlo Park, CA, USA). S1 nuclease treatment was used to detect SSBs as described for Illumina-based sequencing. Per sample, 5–22 $\times$ 10^4 reads were obtained. Long-reads were aligned using an in-house R script based on the pairwiseAlignment function of the Biostrings package (version 2.64.1) with parameters gapOpening = 5, gapExtension = 2 and nucleotide substitution matrix of match = 1, mismatch = −3, baseOnly = TRUE. Only ends with a relative frequency of >3 $\times$ 10^{-5} were used for further analysis.

3. Results

3.1. Transient Hydrogen Peroxide Treatment of HEK 293 Cells Causes Reversible Oxidative Damage of Mitochondrial DNA

In order to model the oxidative damage of mtDNA, we treated HEK 293 cells with 0.5 mM or 1 mM hydrogen peroxide. Due to the presence of the antioxidant pyruvate in the cell growth medium [21], the H_2O_2 concentration rapidly decreased even in the absence

of cells (Figure S2). When cells were present, intrinsic cellular H_2O_2 splitting activities further accelerated the H_2O_2 decay and led to complete removal within 10 min. Thus, our treatment is equivalent to a short H_2O_2 pulse and did not substantially alter cellular viability (>65% at each time point, Figure S3).

To evaluate the integrity of mtDNA after H_2O_2-induced oxidative damage, we performed Southern blotting of agarose electrophoresis separated DNA under non-denaturing conditions (Figure 1). In the presence of ethidium bromide in the agarose gel, intact circular mtDNA migrates as 'supercoiled' faster than full-length (16.5 kb) linear molecules, while nicks, gaps and other alterations can lead to the relaxation of the circular DNA and generate 'open circles' that move slower than the full-length linear mtDNA (Figure 1A,B, lane 1) [9]. Both concentrations of H_2O_2 (0.5 mM and 1 mM) caused an immediate decrease of mtDNA in supercoiled conformation, while the amounts of linear mtDNA and open circle mtDNA increased (Figure 1A,B, lane 2). At 1 mM H_2O_2 concentration, highly fragmented mtDNA was detectable as a smear (Figure 1B, lane 2, Figure 1J). At later time points, the amount of supercoiled mtDNA increased and led to a nearly full recovery after 2 h in 0.5 mM H_2O_2-treated cells and after 6 h at 1 mM H_2O_2 (Figure 1C,E). In parallel, the amount of linear and open-circle species decreased with time (Figure 1A,B, lanes 3–6).

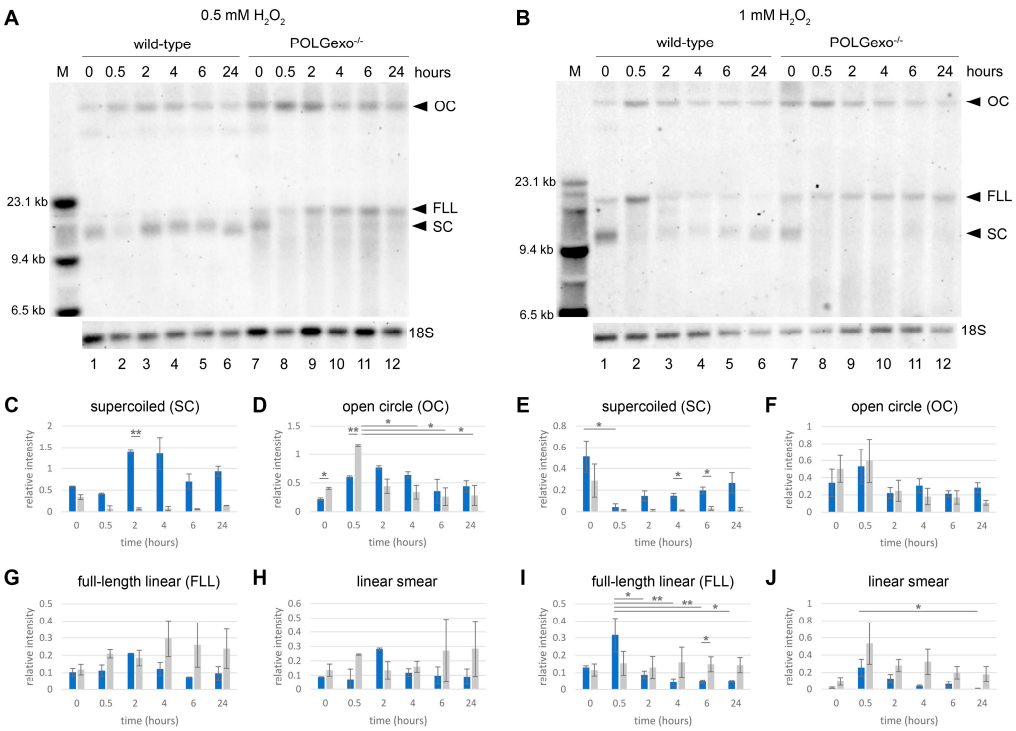

Figure 1. Representative Southern blots of HEK 293 cells treated with (**A**) 0.5 mM H_2O_2, or (**B**) 1 mM H_2O_2. The top label contains "M" molecular weight marker and the time point of the H_2O_2 time course. Lanes 1–6 wild-type HEK 293 cells, lanes 7–12 POLGexo$^{-/-}$ line. Samples have been digested with *Mlu*I for the 18S nuclear loading control while leaving the mtDNA intact. The three main species of mtDNA can be seen: open circle (OC), full-length linear (FLL, 16.5 kb) and supercoiled (SC), as well as a smear of linear mtDNA fragments of smaller sizes. Before H_2O_2 application (lanes 1 and 7), the main conformation of mtDNA is the supercoiled. After 30 min of H_2O_2 treatment (lanes 2 and 8), the supercoiled species is lost, and the other open circle and linear forms increase. The supercoiled is recovered in wild-type cells starting at 2 h after 0.5 mM H_2O_2 treatment and 6 h after 1 mM H_2O_2, but the recovery of the supercoiled is diminished in the POLGexo$^{-/-}$ cells. Note the higher background smear on the POLGexo$^{-/-}$ cell line indicating elevated levels of fragmented linear mtDNA. The quantification of band signal intensities from three different experiments is shown in panels (**C**–**J**).

Blue bars—wild-type cells, gray bars—p.D274A POLG knock-in cell line. Band intensity of the three main mtDNA species (open circle, panels (**D**,**F**); full-length linear, panels (**G**,**I**); and supercoiled, panels (**C**,**E**)) have been quantified, as well as the smear of smaller linear fragments (panels (**H**,**J**)). Data for both cell lines (n = 2 for 0.5 mM and n = 3 for 1.0 mM H_2O_2) are shown as average ± SEM. Significances between time points were assessed by one-way ANOVA and between pairs of wild-type and POLGexo$^{-/-}$ samples by Student's unpaired t-test. **, $p < 0.01$; *, $p < 0.05$. Note that after H_2O_2 treatment of the POLGexo$^{-/-}$ line, a substantial amount of the signal is localized in the smear of fragmented mtDNA, as well as the recovery of supercoiled that is only present in wild-type cells.

Previously, we identified exonuclease-mediated degradation as an important pathway for the clearance of linear mtDNA [12]. In our original HEK 293 cell model, DSBs were introduced by mitochondria-targeted restriction endonucleases, and we found that mtDNA degradation was blocked by the lack of MGME1 exonuclease or by the presence of exonuclease-deficient DNA polymerase γ. In order to evaluate the relevance of the mtDNA degradation pathway in the condition of oxidative damage, we compared the effects of H_2O_2 treatment in wild-type HEK 293 cells with cells harboring the p.D274A mutation in POLG that leads to inactivation of the 3′-5′ exonuclease activity but leaves the polymerase activity intact [12,22]. Similar to wild-type cells, supercoiled mtDNA disappeared after H_2O_2 treatment in POLGexo$^{-/-}$ cells (Figure 1A,B lane 8, Figure 1C,E). However, linear mtDNA (both full-length and highly fragmented) persisted in POLGexo$^{-/-}$ cells and the recovery of supercoiled mtDNA was severely diminished (Figure 1A,B lanes 9–12, Figure 1C,E). Notably, we detected highly fragmented mtDNA species in POLGexo$^{-/-}$ cells even before the H_2O_2 treatment (Figure 1A,B, lane 7), which is in concert with observations in other studies [22,23].

In order to observe a stronger effect of oxidative damage on mtDNA integrity and because cell survival was not strongly affected, the 1 mM H_2O_2 concentration was chosen for further experimentation. We confirmed the transient appearance of mtDNA breaks after the 1 mM H_2O_2 pulse by quantitative real-time PCR. In this approach, amplification efficiencies of a short (115 bp) and a long (1.7 kb) amplicon are compared (Figure 2). A larger observed C_t difference between both amplicons corresponds to a greater amount of mtDNA molecules carrying at least one break within the region spanned by the long amplicon. In line with the Southern blot data presented in Figure 1, the mtDNA damage peaked 30 min after the hydrogen peroxide pulse and disappeared almost 24 h after treatment in wild-type HEK 293 cells (Figure 2, blue bars). In the POLGexo$^{-/-}$ cell line, the mtDNA damage persisted at much higher levels (Figure 2, grey bars). The qPCR amplification on native DNA detects both DSBs and SSBs, the latter at half efficiency because one strand is intact. We aimed to quantify SSBs in 0 h and 24 h samples by digesting DNA with S1 nuclease prior to amplification. S1 nuclease removes single-stranded regions from double-stranded DNA not only at ends but also within the DNA. By the activity of the enzyme, intact strands are cut opposite to nicks and gaps, thus, converting SSBs to DSBs. We estimated the number of SSBs by subtracting non-S1 nuclease-treated values from S1 nuclease-treated values. In opposite to total strand breaks (DSBs + SSBs), SSBs did not show a significant difference either at 0 h (wild-type, 0.76 ± 0.16; POLGexo$^{-/-}$, 0.53 ± 0.01; p = 0.38) or 24 h (wild-type, 0.57 ± 0.18; POLGexo$^{-/-}$, 0.55 ± 0.15; p = 0.96) between wild-type and POLGexo$^{-/-}$ cells. This suggests that SSB repair is unlikely to be influenced by the lack of exonuclease activity of mutant POLG. Note that, using the qPCR method applied in this study, it is not possible to compare amounts of SSBs at the 30 min time point because even non-S1 nuclease-treated values are close to saturation in the POLGexo$^{-/-}$ sample.

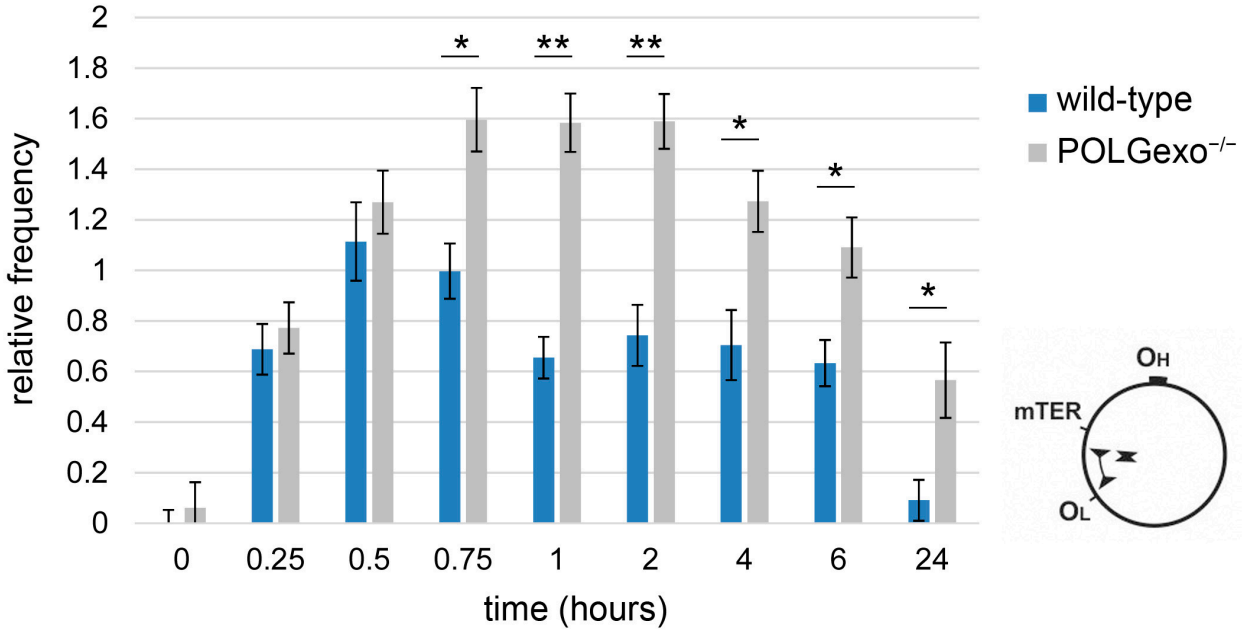

Figure 2. Relative frequency of mtDNA strand breaks after H_2O_2 damage determined by qPCR. Blue, wild-type cells; grey, POLGexo$^{-/-}$ cells. The C_t values of a long amplicon covering a 1.7 kb region in the minor arc were compared with a short amplicon (115 bps). Relative frequencies were calculated as described in the Methods. Samples are averaged for 3 technical replicates for each sample, in addition to 2 biological replicates for time points of 0, 0.5, and 24 h. Error bars, ±SEM. *, $p < 0.05$; **, $p < 0.01$ (Student's *t*-test). Inset, localization of qPCR primers (arrowheads) on the mitochondrial genome (O_H, replication origin H; O_L, replication origin L; mTER, mitochondrial transcription terminator site). The relative frequency of strand breaks increases after the application of H_2O_2, which persists in the POLGexo$^{-/-}$ cells and decreases back to baseline in the wild-type cells.

3.2. Differential Impact of Hydrogen Peroxide Pulse on Mitochondrial and Nuclear DNA Integrity

To identify a large number of mtDNA species, we applied long-read PacBio sequencing to in vitro single-cutter-linearized DNA derived from isolated mitochondria. Although mtDNA was highly enriched in these samples, they always contained traces of nuclear DNA (3–20%). This enabled us to compare the effects of H_2O_2 treatment on the size distribution of DNA fragments of mitochondrial and nuclear origin (Figure 3, left and middle panels). The relative frequency of full-length mtDNA decreased dramatically 30 min after the H_2O_2 pulse (ratio of 0.52 in comparison to 0 h samples, $p = 0.03$), accompanied by higher relative frequencies of fragments in the range of 3–7 kb (ratio of 1.23, $p = 0.006$ for wild-type sample; ratio of 2.36, $p = 0.01$ for POLGexo$^{-/-}$; Figure 3A,D). The fragment size distribution returned almost to the untreated condition in wild-type cells (ratio of 0.96, $p = 0.05$ for short fragments; Figure 3A) 24 h after treatment, and also partially recovered in POLGexo$^{-/-}$ cells (ratio of 1.37 for short fragments, $p < 0.001$; Figure 3D). No such transient decrease in average fragment size after H_2O_2 was observed in nuclear DNA fragments (Figure 3B,E).

Treatment of the DNA samples with S1 nuclease additionally converts SSBs to DSBs. Accordingly, we observed a further increase in DNA fragmentation in both mtDNA and nuclear DNA (Figure 3G,H,J,K). However, again, no elevated frequencies of short nuclear DNA fragments were observed 30 min after H_2O_2 treatment (Figure 3H,K).

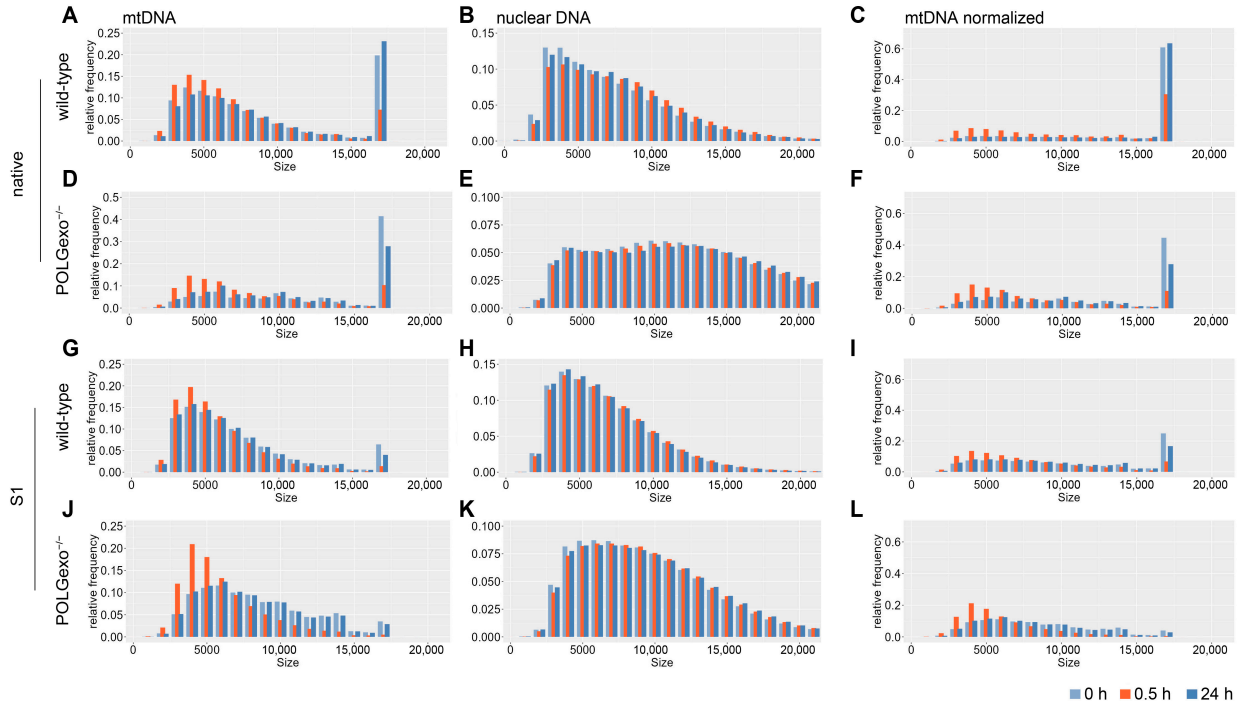

Figure 3. Size distribution of DNA fragments detected by long-read PacBio Sequencing. Panels on the left (**A,D,G,J**) represent fragments that align with the mitochondrial genome. Middle panels (**B,E,H,K**) show non-mitochondrial fragments. Light blue, before H_2O_2 treatment; dark blue, 24 h after treatment; red, 30 min after treatment. Representative experiments of 3 PacBio sequencing experiments are shown. Note that the probability of obtaining large (>15 kb) sequences varies between reactions, as demonstrated by non-mitochondrial sequences (panels (**B**) vs. (**E**)). Therefore, mtDNA fragment frequencies were additionally normalized to the sequencing run that resulted in the highest proportion of large fragments (POLGexo$^{-/-}$, 24 h, in panels (**E**) and (**K**), respectively), which is shown in the right-hand side panels (**C,F,I,L**). Low frequencies of fragments <3 kb are due to size exclusion during library preparation. Note the increased frequency of short mtDNA fragments 30 min after H_2O_2 treatment which is not present in the nuclear DNA.

Surprisingly, the relative frequencies of the full-length mtDNA seemed to be higher in POLGexo$^{-/-}$ cells (Figure 3D) than in wild-type cells (Figure 3A), which clearly contradicts our observations obtained by Southern blotting and qPCR (Figures 1 and 2). An inspection of the size distributions of nuclear DNA fragments revealed that the detection probability of DNA fragments always decreased for larger sizes, and this size bias was different from reaction to reaction (Figure 3B vs. 3E). Therefore, we calculated correction factors for each size bin based on actually observed nuclear DNA sizes in each sample as compared to the sample with the lowest size bias (POLGexo$^{-/-}$, 24 h; Figure 3E,K). These correction factors were then applied to the corresponding mtDNA fragments (Figure 3, right panels). Normalized size distributions showed that over 60% of mtDNA was intact in wild-type cells before H_2O_2 treatment and 24 h after treatment (Figure 3C). However, the frequency of full-length mtDNA was initially lower in POLGexo$^{-/-}$ cells and the recovery 24 h after H_2O_2 treatment was only partial (Figure 3F).

3.3. Increased Amount of DSBs but Not SSBs in POLGexo$^{-/-}$ Cells

Quantification of all deep sequencing-detected ends normalized to average coverage in each sample showed that approximately 2–5% of mtDNA molecules carried DSBs before H_2O_2 treatment in wild-type cells (Figure 4A,B), while the number of SSBs was a magnitude of order higher (Figure 4C,D). In accordance with previous reports [22,23], POLGexo$^{-/-}$ cells already contained a large number of DSBs before H_2O_2 treatment (Figure 4A,B).

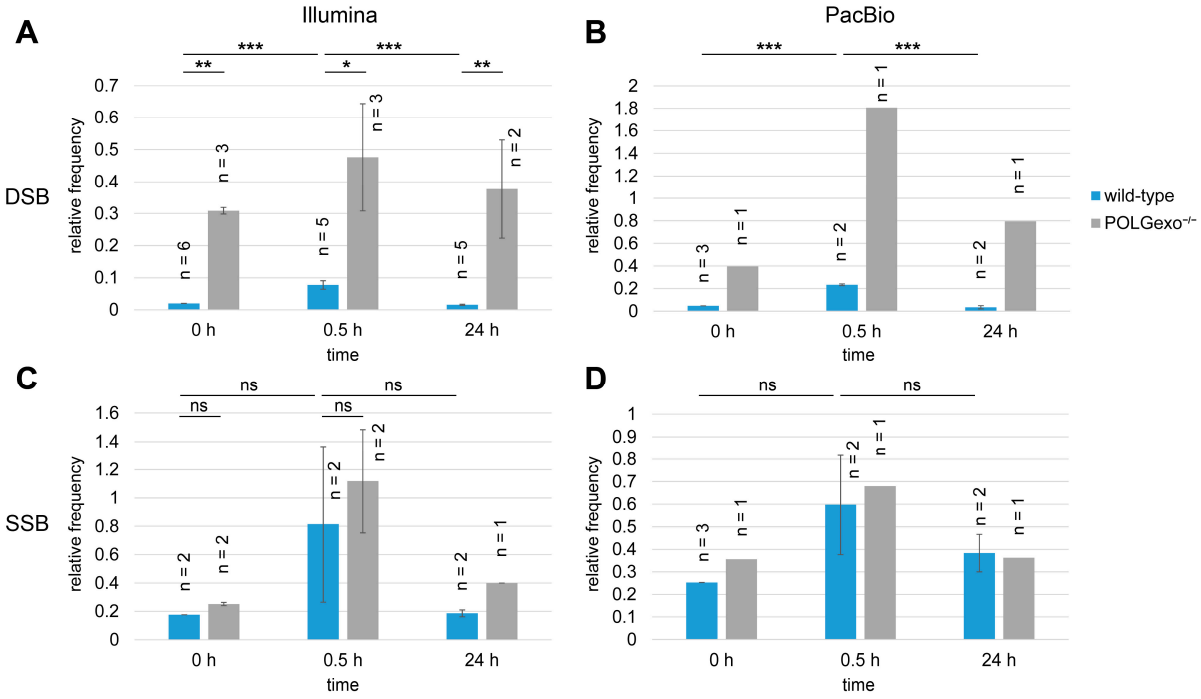

Figure 4. Quantification of mtDNA ends by deep sequencing. Left panels (**A,C**), linker-mediated short-read Illumina sequencing. Right panels (**B,D**), long-read PacBio sequencing. (**A**,**B**), frequency of double-strand breaks (DSBs), (**C**,**D**), frequency of single-strand breaks (SSBs). The amount of SSBs was determined by S1 nuclease treatment and then subtracting frequencies of DSBs. Frequencies are shown relative to average coverages, thus, representing the average number of breaks per mtDNA molecule. Error bars, ±SEM. Significances between time points were assessed by one-way ANOVA and between pairs of wild-type and POLGexo$^{-/-}$ samples by Student's unpaired *t*-test. ***, $p < 0.001$; **, $p < 0.01$; *, $p < 0.05$. DSBs and SSBs increase in all samples after H_2O_2 treatment and decrease after 24 h in wild-type cells. While SSBs behave similarly to the wild-type in the POLGexo$^{-/-}$ cells (**C,D**), DSBs are elevated before H_2O_2 and persist (**A,B**). Note that the increased frequency of SSBs in 0.5 h samples is not significant either in Illumina or PacBio experiments alone. However, when combining values from both types of experiments, 0.5 h samples show a significant ($p = 0.036$) increase compared to 0 h samples but no differences between wild-type and POLGexo$^{-/-}$ cells.

The H_2O_2 pulse led to an approximately 5-fold elevation of DSB frequency in wild-type cells, which was reversed to baseline levels after 24 h. The elevated DSB levels in the POLGexo$^{-/-}$ cell line showed inconsistent changes upon H_2O_2 treatment in the two deep sequencing approaches (Figure 4A,B). The frequency of SSBs was elevated 30 min after H_2O_2 treatment which was reversed after 24 h, although this was not significant due to large variation and the limited number of analyzed samples. No substantial differences in SSBs were observed between wild-type and POLGexo$^{-/-}$ cells.

3.4. Degradation-Specific Sequence Motifs Are Detectable in POLGexo$^{-/-}$ Cells and upon H_2O_2 Damage

In addition to quantification, we aimed to see whether H_2O_2-induced mtDNA ends were associated with specific sequence motifs. Therefore, we determined the relative frequencies of nucleotides at positions relative to the starting or end position of detected mtDNA fragments. Ends were found to be preferentially located proximal to short GC-stretches 30 min after the H_2O_2 pulse, and this pattern was absent before or 24 h after the treatment in wild-type cells (Figure 5). Illumina and PacBio data were consistent. However, in POLGexo$^{-/-}$ cells, mtDNA ends showed a pronounced association with GC-stretches at each time point (Figure 6). These observations show a striking similarity to our previously reported findings obtained from cells in which a DSB was introduced at a single site of the mtDNA by inducibly expressing a mitochondria-targeted restriction endonuclease [12].

Under those conditions, an association of ends with GC-stretches was present in wild-type cells only after 6 h of endonuclease expression but not before or 24 h after induction, while ends in POLGexo$^{-/-}$ cells showed persistent association with GC-stretches. Combining the current results with our previous study, the GC-stretches at ends that appear upon H_2O_2 damage in wild-type HEK 293 cells and that are always present in POLGexo$^{-/-}$ cells are indicative of ongoing linear mtDNA degradation, rather than the original site of DSBs.

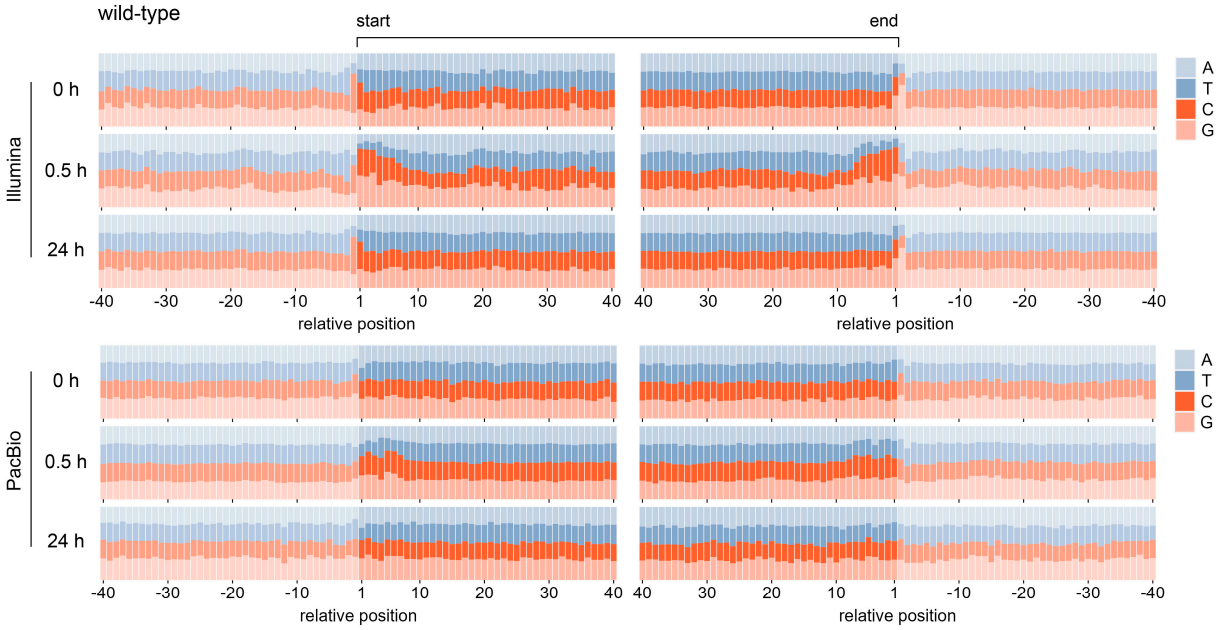

Figure 5. Sequence motifs at the ends of mtDNA fragments detected by deep sequencing in wild-type HEK 293 cells. Nucleotides within a 40 bp distance relative to detected ends were counted. Position-specific nucleotide frequencies were normalized to overall nucleotide frequencies. Upper panels, Illumina sequencing results from natively blunt linker-ligatable mtDNA ends. Lower panels, PacBio sequencing of linear mtDNA. mtDNA samples before treatment, 30 min after H_2O_2 pulse, and 24 h after H_2O_2 were investigated. Ends associated with GC-stretches are present only 30 min after the H_2O_2 but absent before treatment and after 24 h of recovery (cf. Figure 4a in Reference [12]).

3.5. De Novo mtDNA Synthesis Does Not Play a Crucial Role in Short-Term Recovery after H_2O_2 Damage

To determine whether increased mtDNA replication from intact mtDNA molecules contributes to the recovery observed in the wild-type cell line after the H_2O_2 pulse, BrdU incorporation into mtDNA was investigated. In these experiments, 20 µM aphidicolin was added to allow the halting of nuclear DNA replication [18]. Prominent bands appearing during BrdU incorporation were verified as different conformations of the mtDNA by subsequent hybridization with a mitochondria-specific probe (Figure S4). In both wild-type and POLGexo$^{-/-}$ cell lines, BrdU was gradually incorporated into all conformations of mtDNA when applied to the cell growth medium in the absence of H_2O_2, although this incorporation was slightly reduced in the POLGexo$^{-/-}$ cells (Figure 7A,B). The incorporation of BrdU into the mtDNA is consistent with ongoing cell division and accompanying replication of mtDNA to maintain constant mtDNA copy numbers. When BrdU is applied to cells along with H_2O_2, the BrdU incorporation was apparently lower at early time points in both wild-type and POLGexo$^{-/-}$ cells and only became comparable to cells without H_2O_2 treatment after 24 h (Figure 7C,D). These data suggest that the fast recovery of intact mtDNA after H_2O_2 damage observed in the short time frame of 2–6 h does not depend on accelerated de novo mtDNA replication. Conversely, mtDNA replication appears transiently delayed, probably due to the lower amounts of available intact mtDNA templates. Therefore, the fast recovery of supercoiled mtDNA observed after the H_2O_2 pulse in wild-type cells is mainly due to the repair of SSBs.

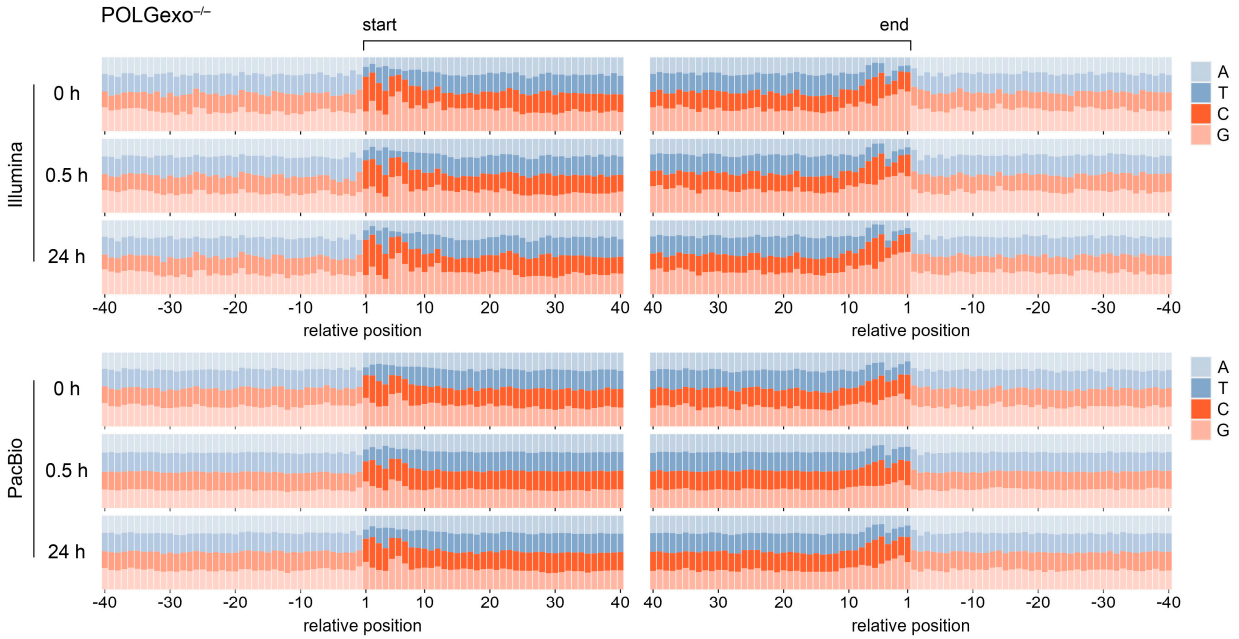

Figure 6. Sequence motifs at the ends of mtDNA fragments detected by deep sequencing in POLGexo$^{-/-}$ cells. Nucleotides within a 40 bp distance relative to detected ends were counted. Position-specific nucleotide frequencies were normalized to overall nucleotide frequencies. Upper panels, Illumina sequencing results from natively blunt linker-ligatable mtDNA ends. Lower panels, PacBio sequencing of linear mtDNA. mtDNA samples before treatment, 30 min after H_2O_2 pulse, and 24 h after H_2O_2 were investigated. Persistent ends in POLGexo$^{-/-}$ cells are associated with GC-stretches (cf. Figure 4d in Reference [12]).

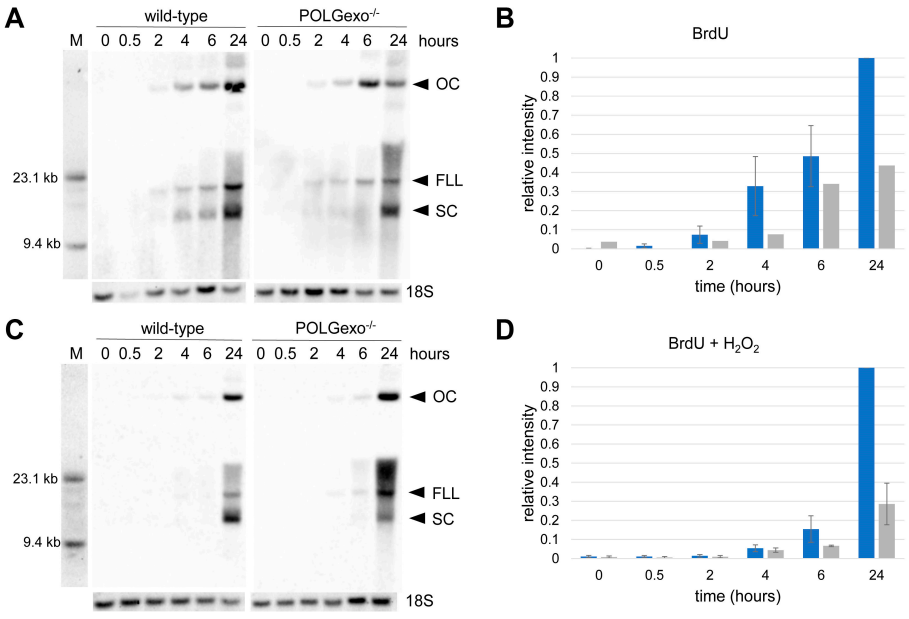

Figure 7. BrdU southern blot and quantification of BrdU incorporation into HEK 293 cell lines. (**A**,**B**): Experiments without hydrogen peroxide addition. (**C**,**D**): Experiments in the presence of 1 mM hydrogen peroxide. Southern blots (**A**,**C**) have been labeled with a BrdU antibody to visualize BrdU-incorporated DNA. "M" is for the molecular weight marker, and time points are indicated. All samples have been digested with *Mlu*I for the 18S nuclear loading control while keeping mtDNA intact. The molecular weight marker and the 18S have been visualized with a DIG-labeled 18S probe.

Blots have been assembled from portions of the same membrane. The three main species of mtDNA can be seen: open circle (OC), full-length linear (FLL), and supercoiled (SC) (see Figure S4 for mtDNA probe confirmation). The large dark cloud smear in the 24 h time points is from nuclear DNA BrdU incorporation due to an incomplete block by aphidicolin. Quantification (**B**,**D**) of the relative intensity of BrdU incorporated into mtDNA as the sum of all three major mtDNA species. Time after BrdU application is on the *x*-axis in hours, and the *y*-axis is the relative intensity of BrdU incorporated into mtDNA. Band intensity is normalized to the 18S loading control and the 24-h control sample. Blue bars—wild-type HEK 293 cells, gray bars—POLGexo$^{-/-}$ cells. Error bars, ±SEM (**B**): n = 4 for wild-type and n = 1 for POLGexo$^{-/-}$. BrdU begins to be incorporated into mtDNA at 2 h in the non-H_2O_2 condition, which is slightly reduced in the POLGexo$^{-/-}$ cells. (**D**): n = 5 for wild-type and n = 2 for POLGexo$^{-/-}$. BrdU is apparently incorporated at a lower rate in the presence of H_2O_2, only reaching comparable amounts to the non-H_2O_2 samples after 24 h (however, the difference between the treatment conditions did not reach statistical significance). The observed rate of BrdU incorporation in the presence of H_2O_2 indicates that increased mtDNA replication is very unlikely to be responsible for the fast recovery of intact mtDNA in wild-type cells after H_2O_2 damage.

4. Discussion

Mitochondrial DNA, packed into dense protein-DNA complexes (nucleoids), is associated with the matrix side of the inner mitochondrial membrane in a highly oxidative environment. The combination of abundant respiratory chain-driven superoxide generation [24,25] and the high amounts of free iron within the mitochondrial matrix [26] has a dangerous potential to generate the extremely reactive hydroxyl radical (•OH). Normally, the superoxide anion is rapidly converted to H_2O_2 by superoxide dismutases (SOD2 in the mitochondrial matrix) as part of the defense against oxidative stress. H_2O_2 is then either further reduced to water by the thioredoxin-2 antioxidant system (in brain mitochondria, [24]) or glutathione peroxidase and catalase (in liver mitochondria, [25,27]) but eventually serves as a potential source for the harmful hydroxyl radical produced in a reaction with free Fe^{2+} (Fenton reaction) [28,29]. The low reactivity of H_2O_2 makes it the only ROS that can travel larger distances within the cell. In fact, H_2O_2 can not only leave mitochondria, but cytosolic H_2O_2 is able to enter mitochondria via an aquaporin-dependent mechanism [30]. Thus, independent of the site of generation, H_2O_2 will likely induce oxidative damage on biomolecules in cellular compartments with high iron content, particularly within mitochondria that are important hubs of cellular iron homeostasis since iron is required for the synthesis of heme and iron-sulfur clusters [2]. In this context, it is important to mention that the intrinsic mitochondrial H_2O_2 splitting activity is not sufficient to cope with the maximal production rates and is highly tissue-specific [25,27].

External hydrogen peroxide has long been used as a model of oxidative damage in cultured cells [31], although its specificity was questioned, and alternative methods of oxidative damage have been investigated [32]. Here we show that, in the presence of pyruvate in the medium, the treatment with 1 mM H_2O_2 is well tolerated by HEK 293 cells, likely due to the fact that H_2O_2 readily degrades in the cell growth medium even in the absence of cells and this decay is accelerated when cells are present. Thus, the addition of H_2O_2 to the medium is transient and leads to a 10-min pulse of oxidative challenge. The concentrations of H_2O_2 that we applied to HEK 293 cells in this study are higher than the ~150 µM that was reported in vivo under the condition of ischemia-reperfusion due to intrinsic respiratory chain-driven superoxide generation [33]. Nevertheless, substantially higher local concentrations can be expected after the activation of plasma membrane NADPH oxidases of microglia or invading immune cells [34,35].

In our model system of HEK 293 cells, hydrogen peroxide induces accumulation of both DSBs and SSBs in mtDNA, which reaches a maximum of half an hour after the H_2O_2 pulse. In contrast, H_2O_2-induced fragmentation of the nuclear genome was not detectable, as demonstrated by the unaltered size distribution of long single-molecule-derived nuclear sequences detected by the PacBio long-read sequencing technique. This is consistent with

the above-mentioned assumption that H_2O_2 can reach various cellular compartments but leads to oxidative damage, primarily in those with high free iron concentrations. Hydroxyl radicals locally generated by the iron-dependent Fenton reaction can attack the sugar backbone of mtDNA [10], leading to SSBs, and likely also to DSBs through a second hit or through replication stalling at SSBs or modified bases. The hydroxyl radical can also oxidize single nucleotides; however, we did not address this question in this study. It has been shown that mitochondrial BER is able to remove oxidized nucleotides from the mtDNA [11]. The excision of the oxidized base and the subsequent removal of the remaining sugar moiety generates a gap, i.e., an SSB, which is then re-sealed by the concerted action of the polymerase activity of POLG, various 5′-3′ exonucleases and, finally, the mitochondrial ligase LIG3. Our data show that SSB repair as part of the BER pathway after oxidative damage is functional both in wild-type and POLGexo$^{-/-}$ cells and that the loss of the 3′-5′ exonuclease activity of POLG does not interfere with the SSB repair. Using our technique to assess SSBs, we cannot distinguish between SSBs on circular and linear mtDNA species. This distinction is hardly relevant in wild-type cells in which the vast majority of mtDNA exists in the form of supercoiled circular DNA. In opposite to this, exonuclease-deficient POLG is known to lead to the accumulation of linear mtDNA species [22,23]. When SSBs on such linear mtDNA molecules are locally repaired, this repair does not generate fully intact supercoiled mtDNA but reduces the number of SSBs on both circular and linear mtDNA.

Wild-type HEK 293 cells not only survive the H_2O_2 pulse but are able to partially recover the integrity of their mitochondrial genomes within hours, as indicated by the reappearance of supercoiled mtDNA species on Southern blots. However, we did not detect any signs of boosted replication in BrdU incorporation assays, which indicates that mtDNA replication does not play a central role in the early phase of recovery from oxidative damage-induced mtDNA breaks.

Unlike the response to SSBs, there was a dramatic difference in the dynamics of generation and clearance of DSBs between wild-type and POLGexo$^{-/-}$ cells. This is not surprising given the fact that we and others demonstrated that the 3′-5′ exonuclease activity of POLG is a central part of the machinery that is responsible for the rapid degradation of linear mtDNA species [12,36,37]. In addition, another hallmark of ongoing mtDNA degradation, a preferential localization of mtDNA ends proximal to GC-stretches, was detected 30 min after oxidative damage. We previously identified such sequence motifs as transient pausing sites of degradation of linear mtDNA [12]. This pattern was absent 24 h after the H_2O_2 pulse in wild-type cells, indicating successful completion of the removal of fragmented mtDNA.

Interestingly, POLGexo$^{-/-}$ cells showed similar sequence patterns of mtDNA ends prior to H_2O_2 damage as well as at 30 min or 24 h after the H_2O_2 pulse. This apparently contradicts our previous finding that the loss of the 3′-5′exonuclease activity of POLG inhibits linear mtDNA degradation [12]. In our previous model of DSB formation, a mitochondria-targeted restriction endonuclease was used to cleave mtDNA at a single position. Although gross degradation was inhibited, both by inactivation of the 3′-5′ exonuclease activity of POLG or knocking out the mitochondrial 5′-3′ exonuclease MGME1, an inspection of the vicinity of the cutting site reveals that, unlike the MGME1 knock-out, exonuclease deficient p.D274A POLG still exhibits a small residual activity of linear mtDNA degradation (cf. Figure 3a in [12]). Of note, the vast majority of linear mtDNA species in POLGexo$^{-/-}$ cells exist independent of the H_2O_2 pulse, and the observed ends represent intermediates of severely impaired degradation of continuously generated linear mtDNA species.

In contrast to previous approaches, which utilized mitochondria-targeted endonucleases to artificially generate double-strand breaks in the mtDNA [12,36], in the present work, we used a pulse with the natural oxidant hydrogen peroxide to induce the generation of mtDNA single-strand and double-strand breaks. After this oxidative insult, the integrity of mtDNA was rapidly restored by fast degradation of linear mtDNA and rapid repair of

single-strand breaks, while mtDNA re-synthesis by replication was identified as a much slower process (Scheme 1).

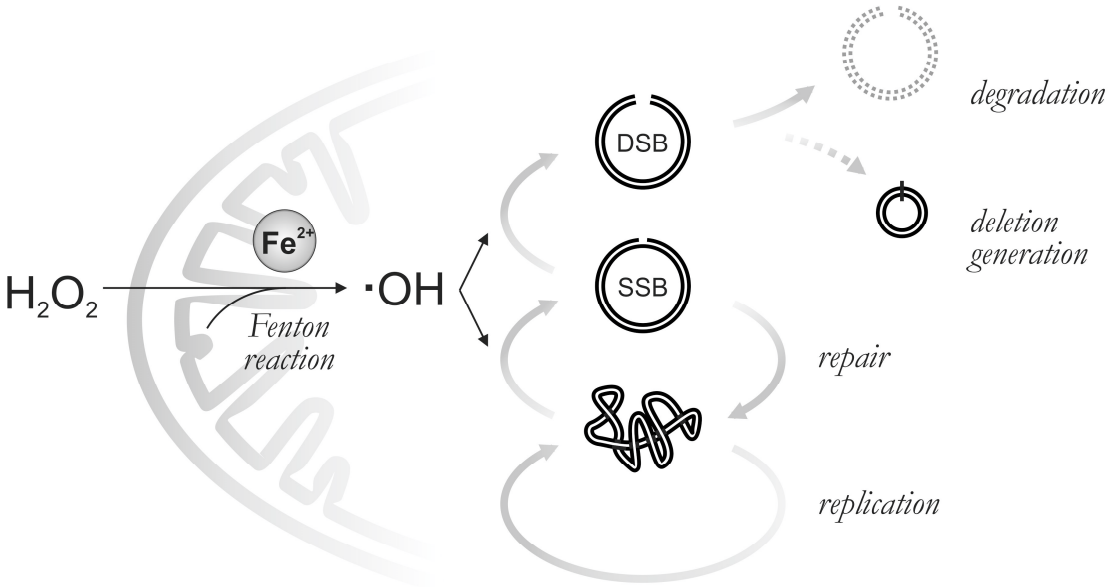

Scheme 1. The fate of mtDNA after oxidative attack by H_2O_2. H_2O_2, independent of the site of its generation, is converted by the Fenton reaction to form the •OH radical, which attacks supercoiled intact mtDNA forming mtDNA molecules containing SSBs. These are either repaired or converted to molecules with DSBs. Linearized mtDNA molecules are rapidly degraded to prevent the formation of harmful somatic mtDNA deletions by non-homologous end joining.

Rapid degradation of linear mtDNA is, therefore, an important quality control pathway of mtDNA because it precludes the potential formation of harmful mtDNA deletions from accumulating linear mtDNA molecules by non-homologous end-joining [36]. However, under conditions when the degradation of linear mtDNA is not efficient enough to completely remove all linear mtDNA fragments, somatic mtDNA deletion generation could result (cf. Scheme 1). That could explain findings of low-level mtDNA deletions in pathological brain tissue affected by inflammation [38,39] since invading immune cells or activated microglia have been identified as potential sources of hydrogen peroxide [34,35].

5. Conclusions

Our data highlight the interplay and timing of repair, degradation, and re-synthesis of mtDNA after transient oxidative damage. Furthermore, the results demonstrate the essential role of the rapid linear mtDNA degradation pathway for mtDNA quality control to avoid somatic mtDNA deletion formation.

Supplementary Materials: The following supporting information can be downloaded at: https://www.mdpi.com/article/10.3390/antiox12051087/s1, Figure S1: Sequencing chromatogram showing the genotype of the POLGexo− HEK 293 cells line; Figure S2: H_2O_2 concentration decay in presence and absence of cells; Figure S3: Viability of HEK 293 cell lines after a 1 mM H_2O_2 pulse; Figure S4: BrdU incorporation into wild-type cells in normal medium and the presence of 1mM H_2O_2 (A), and the same blot developed with a MT-ND5 probe (B).

Author Contributions: Conceptualization, W.S.K. and G.Z.; methodology, J.A., K.B. and K.K.; software, G.Z.; formal analysis, G.T., A.P.K. and A.M.S.; investigation, G.T., A.M.S., A.P.K., J.A., K.B. and V.P.; writing—original draft preparation, W.S.K.; writing—review and editing, W.S.K. and G.Z.; visualization, G.Z.; supervision, W.S.K. and K.K.; funding acquisition, G.Z., W.S.K. and K.K. All authors have read and agreed to the published version of the manuscript.

Funding: This research was funded by the Deutsche Forschungsgemeinschaft (DFG, German Research Foundation): ZS 99/3-2 and ZS 99/4-1 to G.Z., KU 911/21-2 and KU 911/22-1 to W.S.K. This

work was supported by the DFG Research Infrastructure West German Genome Center (407493903) as part of the Next Generation Sequencing Competence Network (project 423957469). NGS analyses were carried out at the West German Genome Center, and production sites in Cologne and Düsseldorf. A.M.S. was supported by a scholarship from KAAD.

Institutional Review Board Statement: Not applicable.

Informed Consent Statement: Not applicable.

Data Availability Statement: The data presented in this study are available in the article and Supplementary Materials.

Acknowledgments: The authors thank Susanne Beyer, Kerstin Hallmann (Bonn) and Anja Schuster (Düsseldorf) for the excellent technical assistance. Computational infrastructure and support for PacBio sequencing were provided by the Centre for Information and Media Technology at Heinrich Heine University Düsseldorf.

Conflicts of Interest: The authors declare no conflict of interest.

References

1. Alexeyev, M.F. Is there more to aging than mitochondrial DNA and reactive oxygen species? *FEBS J.* **2009**, *276*, 5768–5787. [CrossRef]
2. Levi, S.; Rovida, E. The role of iron in mitochondrial function. *Biochim. Biophys. Acta* **2009**, *1790*, 629–636. [CrossRef]
3. Chance, B.; Sies, H.; Boveris, A. Hydroperoxide metabolism in mammalian organs. *Physiol. Rev.* **1979**, *59*, 527–605. [CrossRef]
4. Itsara, L.S.; Kennedy, S.R.; Fox, E.J.; Yu, S.; Hewitt, J.J.; Sanchez-Contreras, M.; Cardozo-Pelaez, F.; Pallanck, L.J. Oxidative stress is not a major contributor to somatic mitochondrial DNA mutations. *PLoS Genet.* **2014**, *10*, e1003974. [CrossRef]
5. Szczepanowska, K.; Trifunovic, A. Origins of mtDNA mutations in ageing. *Essays Biochem.* **2017**, *61*, 325–337.
6. Kauppila, T.E.S.; Kauppila, J.H.K.; Larsson, N.G. Mammalian mitochondria and aging: An update. *Cell Metab.* **2017**, *25*, 57–71. [CrossRef]
7. Gustafsson, C.M.; Falkenberg, M.; Larsson, N.G. Maintenance and Expression of Mammalian Mitochondrial DNA. *Annu. Rev. Biochem.* **2016**, *85*, 133–160. [CrossRef]
8. Sanchez-Contreras, M.; Sweetwyne, M.T.; Kohrn, B.F.; Tsantilas, K.A.; Hipp, M.J.; Schmidt, E.K.; Fredrickson, J.; Whitson, J.A.; Campbell, M.D.; Rabinovitch, P.S.; et al. A replication-linked mutational gradient drives somatic mutation accumulation and influences germline polymorphisms and genome composition in mitochondrial DNA. *Nucleic Acids Res.* **2021**, *49*, 11103–11118. [CrossRef]
9. Zsurka, G.; Peeva, V.; Kotlyar, A.; Kunz, W.S. Is There Still Any Role for Oxidative Stress in Mitochondrial DNA-Dependent Aging? *Genes* **2018**, *9*, 175. [CrossRef]
10. Dizdaroglu, M.; Jaruga, P. Mechanisms of free radical-induced damage to DNA. *Free Radic. Res.* **2012**, *46*, 382–419. [CrossRef]
11. Alencar, R.R.; Batalha, C.M.P.F.; Freire, T.S.; de Souza-Pinto, N.C. Enzymology of mitochondrial DNA repair. *Enzymes* **2019**, *45*, 257–287.
12. Peeva, V.; Blei, D.; Trombly, G.; Corsi, S.; Szukszto, M.J.; Rebelo-Guiomar, P.; Gammage, P.A.; Kudin, A.P.; Becker, C.; Altmüller, J.; et al. Linear mitochondrial DNA is rapidly degraded by components of the replication machinery. *Nat. Commun.* **2018**, *9*, 1727. [CrossRef]
13. Shokolenko, I.; Venediktova, N.; Bochkareva, A.; Wilson, G.L.; Alexeyev, M.F. Oxidative stress induces degradation of mitochondrial DNA. *Nucleic Acids Res.* **2009**, *37*, 2539–2548. [CrossRef]
14. Shokolenko, I.N.; Alexeyev, M.F. Mitochondrial DNA: A disposable genome? *Biochim. Biophys. Acta* **2015**, *1852*, 1805–1809. [CrossRef]
15. Malinska, D.; Kudin, A.P.; Bejtka, M.; Kunz, W.S. Changes in mitochondrial reactive oxygen species synthesis during differentiation of skeletal muscle cells. *Mitochondrion* **2012**, *12*, 144–148. [CrossRef]
16. Trounce, I.A.; Kim, Y.L.; Jun, A.S.; Wallace, D.C. Assessment of mitochondrial oxidative phosphorylation in patient muscle biopsies, lymphoblasts, and transmitochondrial cell lines. *Methods Enzymol.* **1996**, *264*, 484–509. [CrossRef]
17. Hussain, M.; Mohammed, A.; Saifi, S.; Khan, A.; Kaur, E.; Priya, S.; Agarwal, H.; Sengupta, S. MITOL-dependent ubiquitylation negatively regulates the entry of PolγA into mitochondria. *PLoS Biol.* **2021**, *19*, e3001139. [CrossRef]
18. Davis, A.F.; Clayton, D.A. In situ localization of mitochondrial DNA replication in intact mammalian cells. *J. Cell Biol.* **1996**, *135*, 883–893. [CrossRef]
19. Magnusson, J.; Orth, M.; Lestienne, P.; Taanman, J.W. Replication of mitochondrial DNA occurs throughout the mitochondria of cultured human cells. *Exp. Cell Res.* **2003**, *289*, 133–142. [CrossRef]
20. Tullman, J.; Guntas, G.; Dumont, M.; Ostermeier, M. Protein switches identified from diverse insertion libraries created using S1 nuclease digestion of supercoiled-form plasmid DNA. *Biotechnol. Bioeng.* **2011**, *108*, 2535–2543. [CrossRef]
21. Guarino, V.A.; Oldham, W.M.; Loscalzo, J.; Zhang, Y.Y. Reaction rate of pyruvate and hydrogen peroxide: Assessing antioxidant capacity of pyruvate under biological conditions. *Sci. Rep.* **2019**, *9*, 19568. [CrossRef]

22. Trifunovic, A.; Wredenberg, A.; Falkenberg, M.; Spelbrink, J.N.; Rovio, A.T.; Bruder, C.E.; Bohlooly, Y.M.; Gidlöf, S.; Oldfors, A.; Wibom, R.; et al. Premature ageing in mice expressing defective mitochondrial DNA polymerase. *Nature* **2004**, *429*, 417–423. [CrossRef]
23. Hämäläinen, R.H.; Landoni, J.C.; Ahlqvist, K.J.; Goffart, S.; Ryytty, S.; Rahman, M.O.; Brilhante, V.; Icay, K.; Hautaniemi, S.; Wang, L.; et al. Defects in mtDNA replication challenge nuclear genome stability through nucleotide depletion and provide a unifying mechanism for mouse progerias. *Nat. Metab.* **2019**, *1*, 958–965. [CrossRef]
24. Kudin, A.P.; Bimpong-Buta, N.Y.; Vielhaber, S.; Elger, C.E.; Kunz, W.S. Characterization of superoxide-producing sites in isolated brain mitochondria. *J. Biol. Chem.* **2004**, *279*, 4127–4135. [CrossRef]
25. Kudin, A.P.; Malinska, D.; Kunz, W.S. Sites of generation of reactive oxygen species in homogenates of brain tissue determined with the use of respiratory substrates and inhibitors. *Biochim. Biophys. Acta* **2008**, *1777*, 689–695. [CrossRef]
26. Petrat, F.; Weisheit, D.; Lensen, M.; de Groot, H.; Sustmann, R.; Rauen, U. Selective determination of mitochondrial chelatable iron in viable cells with a new fluorescent sensor. *Biochem. J.* **2002**, *362*, 137–147. [CrossRef]
27. Kudin, A.P.; Augustynek, B.; Lehmann, A.K.; Kovács, R.; Kunz, W.S. The contribution of thioredoxin-2 reductase and glutathione peroxidase to H(2)O(2) detoxification of rat brain mitochondria. *Biochim. Biophys. Acta* **2012**, *1817*, 1901–1906. [CrossRef]
28. Halliwell, B.; Gutteridge, J.M.C. Role of Free Radicals and Catalytic Metal Ions in Human Disease. *Methods Enzymol.* **1990**, *186*, 1–85.
29. Henle, E.S.; Han, Z.; Tang, N.; Rai, P.; Luo, Y.; Linn, S. Sequence-specific DNA cleavage by Fe^{2+}-mediated fenton reactions has possible biological implications. *J. Biol. Chem.* **1999**, *274*, 962–971. [CrossRef]
30. Henzler, T.; Steudle, E. Transport and metabolic degradation of hydrogen peroxide in Chara corallina: Model calculations and measurements with the pressure probe suggest transport of H2O2 across water channels. *J. Exp. Bot.* **2000**, *51*, 2053–2066. [CrossRef]
31. Kaneko, M.; Inoue, F. The sensitivity to DNA single strand breakage in mitochondria, but not in nuclei, of Chinese hamster V79 and variant cells correlates with their cellular sensitivity to hydrogen peroxide. *Toxicol. Lett.* **1998**, *99*, 15–22. [CrossRef] [PubMed]
32. Goffart, S.; Tikkanen, P.; Michell, C.; Wilson, T.; Pohjoismäki, J. The Type and Source of Reactive Oxygen Species Influences the Outcome of Oxidative Stress in Cultured Cells. *Cells.* **2021**, *10*, 1075. [CrossRef] [PubMed]
33. Hyslop, P.A.; Zhang, Z.; Pearson, D.V.; Phebus, L.A. Measurement of striatal H_2O_2 by microdialysis following global forebrain ischemia and reperfusion in the rat: Correlation with the cytotoxic potential of H_2O_2 in vitro. *Brain Res.* **1995**, *671*, 181–186. [CrossRef]
34. Claude, J.; Linnartz-Gerlach, B.; Kudin, A.P.; Kunz, W.S.; Neumann, H. Microglial CD33-related Siglec-E inhibits neurotoxicity by preventing the phagocytosis-associated oxidative burst. *J. Neurosci.* **2013**, *33*, 18270–18276. [CrossRef]
35. Simpson, D.S.A.; Oliver, P.L. ROS Generation in Microglia: Understanding Oxidative Stress and Inflammation in Neurodegenerative Disease. *Antioxidants* **2020**, *9*, 743. [CrossRef] [PubMed]
36. Nissanka, N.; Bacman, S.R.; Plastini, M.J.; Moraes, C.T. The mitochondrial DNA polymerase gamma degrades linear DNA fragments precluding the formation of deletions. *Nat. Commun.* **2018**, *9*, 2491. [CrossRef]
37. Medeiros, T.C.; Thomas, R.L.; Ghillebert, R.; Graef, M. Autophagy balances mtDNA synthesis and degradation by DNA polymerase POLG during starvation. *J. Cell Biol.* **2018**, *217*, 1601–1611. [CrossRef]
38. Volmering, E.; Niehusmann, P.; Peeva, V.; Grote, A.; Zsurka, G.; Altmüller, J.; Nürnberg, P.; Becker, A.J.; Schoch, S.; Elger, C.E.; et al. Neuropathological signs of inflammation correlate with mitochondrial DNA deletions in mesial temporal lobe epilepsy. *Acta Neuropathol.* **2016**, *132*, 277–288. [CrossRef]
39. Campbell, G.R.; Kraytsberg, Y.; Krishnan, K.J.; Ohno, N.; Ziabreva, I.; Reeve, A.; Trapp, B.D.; Newcombe, J.; Reynolds, R.; Lassmann, H.; et al. Clonally expanded mitochondrial DNA deletions within the choroid plexus in multiple sclerosis. *Acta Neuropathol.* **2012**, *124*, 209–220. [CrossRef]

Disclaimer/Publisher's Note: The statements, opinions and data contained in all publications are solely those of the individual author(s) and contributor(s) and not of MDPI and/or the editor(s). MDPI and/or the editor(s) disclaim responsibility for any injury to people or property resulting from any ideas, methods, instructions or products referred to in the content.